ACS SENSORS

pubs.acs.org/acssensors Article

Accurate Isolation of Circulating Tumor Cells via a Heterovalent DNA Framework Recognition Element-Functionalized Microfluidic Chip

Yan Liu, Zhun Lin, Ziwei Zheng, Yuanqing Zhang,* and Lingling Shui*

Cite This: *ACS Sens.* 2022, 7, 666−673 Read Online

ACCESS | Metrics & More | Article Recommendations | Supporting Information

ABSTRACT: Detection of circulating tumor cells (CTCs) has provided a noninvasive and efficient approach for early diagnosis, treatment, and prognosis of cancer. However, efficient capture of CTCs in the clinical environment is very challenging because of the extremely rare and heterogeneous expression of CTCs. Herein, we fabricated a multimarker microfluidic chip for the enrichment of heterogeneous CTCs from peripheral blood samples of breast cancer patients. The multimarker aptamer cocktail DNA nanostructures (TP-multimarker) were modified on a deterministic lateral displacement (DLD)-patterned microfluidic chip to enhance the capture efficiency through the size selection effect of DLD arrays and the synergistic effect of multivalent aptamers. As compared to a monovalent aptamer-modified chip, the multimarker chip exhibits enhanced capture efficiency toward both high and low epithelial cell adhesion molecule expression cell lines, and the DNA nanostructure-functionalized chip enables the accurate capture of different phenotypes of CTCs. In addition, the DNA nanoscaffold makes nucleases more accessible to the aptamers to release cells with molecular integrity and outstanding cell viability.

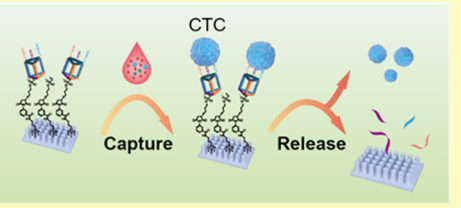

KEYWORDS: *circulating tumor cells, microfluidic chip, aptamer cocktail, DNA triangular prism nanostructure, synergistic effect, biosensor*

Cancer is the second leading cause of death worldwide,[1] with 90% of cancer-related deaths linked to tumor metastasis and spread.[2] In the process of tumor metastasis, tumor cells shed from the primary tumor site into the bloodstream and eventually form secondary tumors through invasion and diffusion of these circulating tumor cells (CTCs).[3,4] The detection and analysis of CTCs, which are representative of this metastatic disease, play an important role in tumor diagnosis, treatment guidance, as well as prognosis.[5] However, detection and enumeration of CTCs with high efficiency are a severe challenge because of their extremely low abundance, comprising as few as 1−10 CTCs per 10 mL of blood.[3]

Currently, the CTC enrichment strategy can be broadly classified into antigen-dependent isolation and label-free isolation (cell size, deformability, or density, etc.).[6−8] Positive sorting of CTCs by antibody-mediated adhesion to CTCs, especially epithelial cell adhesion molecules (EpCAMs), is currently the most commonly used method.[9] However, CTCs would exhibit partial down-regulation of the expression of epithelial cell-specific molecules and obtained mesenchymal characteristics after undergoing epithelial to mesenchymal transition (EMT) during tumor progression.[10] In this context, homo-positive marker-based isolation is hampered by inefficiency, and information reflecting disease progression would be lost to some extent. On the other hand, antibody-based enrichment methods make it difficult for CTCs to be released for subsequent analysis, and the destruction of the antibody−cell interaction for cell release will lead to cell damage.

To date, many methods based on the cocktail of multiple ligands have been developed to accurately capture heterogeneous CTCs. By modifying different aptamers on the substrate, the synergy of aptamers has successfully achieved efficient capture of heterogeneous CTCs.[11] Aptamers are oligonucleotides that are spontaneously folded into complex three-dimensional (3D) shapes to mimic antibodies and bind to specific targets with high affinity.[12] Compared with antibodies, aptamers have the unique advantages of physical stability, low cost, and easy modification.[13] Moreover, the interaction between aptamers and cells can be gently destroyed by nuclease degradation so that the cells can be released and used for downstream analysis.[14] However, the surface assembly of the aptamers is affected by many factors, including the electrostatic repulsion between the chains,[15] the nonspecific interaction between the aptamer and the substrate surface,[16] and the strong interchain entanglement,[17] which limit the ability of the aptamer to interact with the antigen expressed on

Received: December 22, 2021
Accepted: January 26, 2022
Published: February 3, 2022

Scheme 1. Working Principle of the TP-Multimarker Chip: (A) Diagram for the Purification of Heterogeneous CTCs by the TP-Multimarker Chip; (B) Working Principle of the Heterovalent Capture and Release on the Multimarker Nanointerface

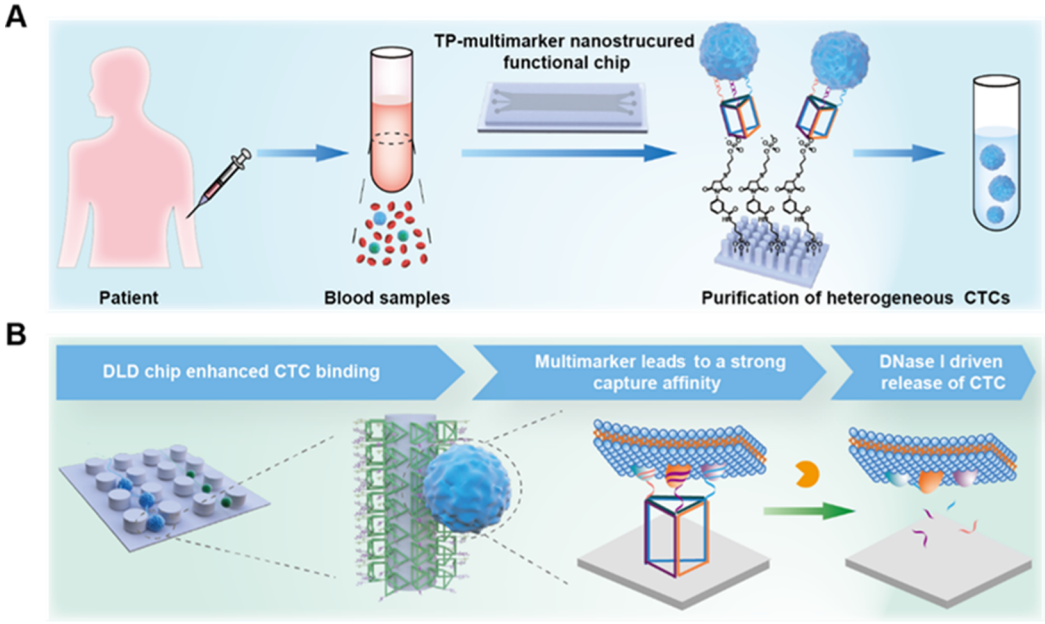

the CTC surface.[18] The ordered spatial orientation of aptamer probes has a great influence on the recognition process. Our previous research has developed and validated a multimarker DNA nanosynapse for CTC detection and separation,[19] with DNA nanostructures allowing aptamer probes to extend toward the solution phase to obtain a highly ordered nanometer-scale precision recognition interface.

Herein, we constructed a multimarker microfluidic chip based on a DNA nanoframework with multiple aptamers. A highly ordered microfluidic nanointerface is fabricated using precisely adjustable 3D DNA nanostructures to accurately capture heterogeneous CTCs. We constructed a triangular prism (TP) DNA nanostructure as a scaffold, and multiple aptamers can pair with the three sides of the upper surface of the TP. The three vertices at the bottom of the TP are anchored as footholds on a microfluidic chip with a deterministic lateral displacement (DLD) micropillar array, forming a nanointerface that efficiently interacts with the target cells (Scheme 1). The cylindrical micropillar array geometric design is applied to the microfluidic chip based on the DLD principle, which improves the collision efficiency between CTCs and micropillars while minimizing the collision between other blood cells and micropillars.[20] The rigid TP DNA nanostructure as a scaffold allows three different aptamers to be controllably arranged in a highly ordered and vertical manner,[17] which is conducive to the interaction between the multimarker aptamers and the surface of the heterogeneous CTCs. Meanwhile, the rigid DNA nanostructure provides reasonable spatial spacing on the interface,[21] making the nuclease more accessible to degrade the aptamers, thereby realizing the efficient release of the captured cells. With its excellent performance of efficiently capturing reduced EpCAM-expressing CTCs in clinical samples, the TP-multimarker microfluidic chip is expected to provide an efficient and reliable strategy for liquid biopsy.

RESULTS AND DISCUSSION

Synthesis and Characterization of the TP-Multimarker Nanostructure. The TP-multimarker was prepared according to traditional DNA annealing self-assembly (Figure S1). Briefly, three thiol-modified scaffold oligonucleotides were annealed to form the TP nanostructure, with three aptamer strands targeting the surface marker [EpCAM, human epidermal growth factor receptor 2 (HER2), and epidermal growth factor receptor (EGFR)] anchored to the vertices of TP. The DNA nanoscaffold was designed to contain rigid edges of 20 base pairs and connected to the aptamers by 3 longer fragments containing aptamer sequences and a linker subpart complementary with the upper edge of the nanostructure. Since the substances on the cell membrane were mobile laterally,[22] proteins could be closed in proximity and allow the TP-multimarker to achieve synergistic recognition on the cell membrane surface.[19] The stepwise assembly of the TP-multimarker nanostructure was characterized by agarose gel electrophoresis analysis (Figure S2A). The mobility of electrophoretic bands decreased with the gradual addition of DNA strands, indicating the successful formation of the TP-multimarker (yield ~ 82.29%, Figure S2B). Additionally, atomic force microscopy (AFM) images confirmed the construction of the nanostructure and show the size and morphology of the TP-multimarker (Figure S3).

Fabrication of a DNA Nanoscaffold Functional Chip. Based on the previous demonstration of DLD chips, where the size-selective interaction of DLD arrays mediated the purification of CTCs with a larger cell size than normal blood cells,[23] we explored the combination of DLD arrays with a multimarker DNA nanostructure recognition unit for the isolation of heterogeneous CTCs. The chip surface was functionalized by the TP-multimarker based on widely used silane chemistry to obtain a DNA nanoscopic interface.[24] After plasma cleaning and silanization with (3-aminopropyl)-trimethoxysilane (APTES), the terminal amino group of silanized PDMS was cross-linked to the thiol-modified TP-multimarker through m-maleimidobenzoyl-N-hydroxysuccini-

https://doi.org/10.1021/acssensors.1c02692
ACS Sens. 2022, 7, 666−673

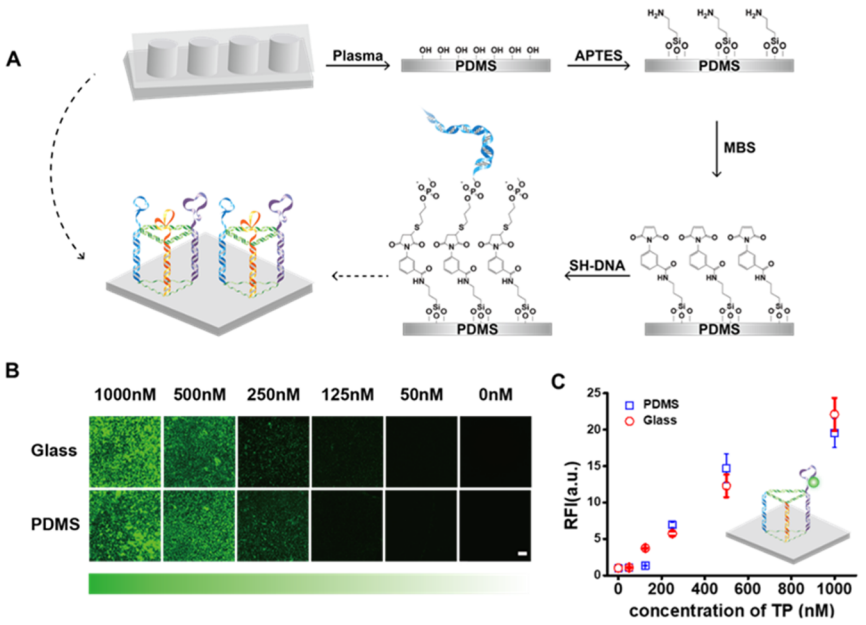

Figure 1. Surface modification and verification of the TP-multimarker chip. (A) Surface chemical modification of the TP-multimarker chip. One FAM-labeled aptamer was assembled into the TP nanostructure to light up the channels. (B) Representative fluorescence images and (C) corresponding fluorescence quantification of DNA nanostructured glass substrates and PDMS substrates, respectively; scale bar = 50 μm.

mide ester (MBS) to generate a DNA-coated microchannel (Figure 1A). To validate surface functionalization, we first used a 6-carboxyfluorescein (FAM)-labeled EpCAM aptamer assembled into the TP nanostructure to light up the channels (Figure S4A). As the chips consisted of glass substrates and PDMS, the glass substrates underwent the same modification process, and representative fluorescence information of glass and PDMS surfaces were collected both before and after DNA assembly (Figure 1B,C). These fluorescence data confirm the successful surface modification. To further observe the tendency of DNA modification on the surface, we modified the chip with TP nanostructures, in which 1/10 of TPs contained an aptamer labeled by FAM. Higher local modification of the DNA nanostructure was observed on the surface of the channel micropillar (Figure S4B), which is beneficial to capturing CTC in the chip. We speculate that this is due to the larger specific surface area of the micropillars and hence has a higher reaction efficiency.

Optimization of Cell Capture Using Artificial CTC Samples. To optimize the capture efficiency of the microfluidic chips, artificial samples were prepared by spiking 500 DiI-labeled positive cells (breast cancer cell lines MCF-7 and MAD-MB-231 with high and low EpCAM expression, respectively) into 10^5 DiO-labeled negative cells (T-lymphocyte cell line Jurkat) in PBS buffer or whole blood (Figure S5A). The artificial samples were introduced into the chips and captured by the TP-multimarker nanostructured microchannels (Figure S5B). We first evaluated the effect of flow rates (0.2, 0.3, 0.4, 0.5 mL/h) on CTC capture efficiency in PBS buffer, and an optimal flow rate of 0.2 mL/h was identified (Figure S6). To explore the role of the DNA nanointerface in the microfluidic chip for enhancing the capture efficiency, we constructed three types of DNA nanointerface: Aptamer-EpCAM chip (Aptamer chip), TP-3EpCAMs chip, and TP-multimarker chip (Figure 2A). TP served as a molecular scaffold, achieving a better binding capacity of the aptamer probe in a spatially homogeneous orderly upright arrangement, while individual aptamer strands existed in interchain entanglement, limiting the interaction with the surface antigen. As hypothesized, the TP-3EpCAMs chip and TP-multimarker chip showed a comparable capture efficiency toward the high EpCAM-expressed cell line MCF-7, which improved by ~50% as compared to the Aptamer chip. This could be attributed to the orderly arrangement of the DNA nanointerface, effectively enhancing the multivalent binding between aptamers and the cell membrane. In addition, the dimerization of HER2 and EGFR could also contribute to the multivalent combination.[25] However, the TP-3EpCAMs chip has shown a limited capture efficiency (67.37%) toward the triple-negative breast cancer cell line MDA-MB-231, which were characterized by low expression of EpCAM, HER2, and EGFR. Correspondingly, the yield of MDA-MB-231 captured by the TP-multimarker chip (90.23%) was higher than those of other methods (Figure 2B). The CTC capture performance recorded for the multimarker cocktail DNA nanostructure exceeded the rest of the groups. Moreover, T-lymphocyte cell line Jurkat cells as the model leukocytes exhibited less than 10% cell residue after the capture process on account of the lack of the EpCAM biomarker expression.

We further explored the potential of the TP-multimarker chip for clinical sample analysis by investigating the capture performance in blood. The whole blood artificial samples were prepared by spiking 500 cells in the blood samples from healthy donors. As shown in Figure 2C, the capture performance of the TP-multimarker chip remained exceeded when compared to the TP-3EpCAMs chip and Aptamer chip as the capture efficiencies of MCF-7 and MDA-MB-231 all surpassed 90%, while the TP-3EpCAMs chip only captured about 63% of MDA-MB-231 and the Aptamer chip exhibited a low capture efficiency toward both MCF-7 (44.41%) and MDA-MB-231 (42.23%). Of note, the nonspecific absorption of white blood cells (WBCs) in the whole blood artificial samples was only 0.04% (Figure S7), indicating that the capture of CTCs by the TP-multimarker had high specificity.

https://doi.org/10.1021/acssensors.1c02692
ACS Sens. 2022, 7, 666−673

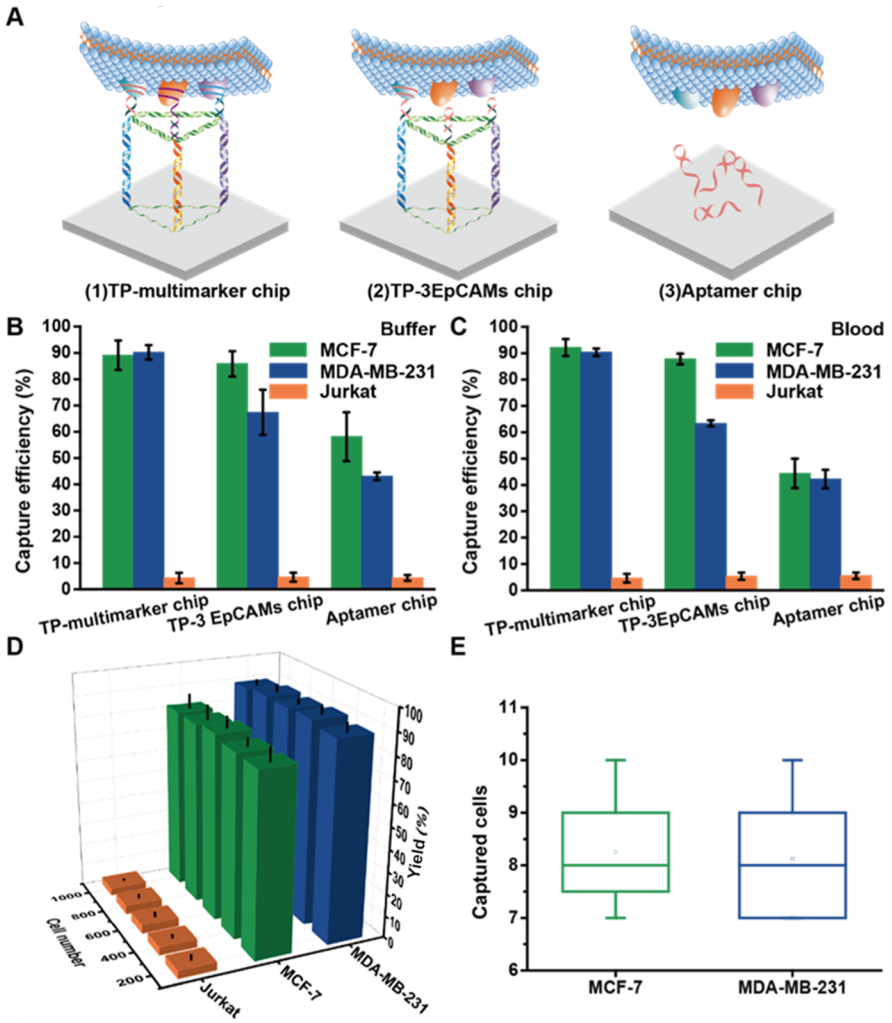

Figure 2. (A) Schematic diagrams of different DNA nanostructure-functionalized interfaces. (B) Capture efficiency of positive cells (MCF-7 and MDA-MB-231) and negative cells (Jurkat) by the TP-multimarker chip, TP-3EpCAMs chip, and Aptamer chip in PBS buffer. (C) Capture efficiency of positive cells (MCF-7 and MDA-MB-231) and negative cells (Jurkat) by the TP-multimarker chip, TP-3EpCAMs chip, and Aptamer chip in whole blood. Cell capture efficiency toward different cell lines of (D) 200−1000 or (E) 10 cells by the TP-multimarker chip.

After determining the optimal conditions of the TP-multimarker chip to capture the CTCs, we next proceed to evaluate the enrichment performance of the TP-multimarker chip in a series of artificial samples. Various numbers of DiI-labeled cells (ranging from 200 to 1000 cells) were fed into the TP-multimarker chip to measure their capture efficiency. As shown in Figure 2D, the TP-multimarker exhibits a high capture efficiency toward both the high expression of EpCAM cell line MCF-7 and the low expression of EpCAM cell line MDA-MB-231. Moreover, to simulate the rarity of CTCs in peripheral blood, 10 cells of different phenotypes were spiked into PBS buffer, and the average capture efficiency reached above 80% (Figure 2E).

We further evaluated the performance of CTC release in the DNA nanostructured chip. An effective and harmless release of CTCs is important for downstream analysis, and several release strategies have been implemented in aptamer-based microfluidic chip devices, including redox reaction,[26] complementary sequence hybridization,[27] and nuclease degradation.[28] These methods are often hindered by steric hindrance or the local overcrowding effect, resulting in a limited CTC release efficiency. Herein, the TP DNA nanoscaffold allows the TP-multimarker to be controllably arranged on the interface, so this makes the nuclease (DNase I) more accessible to the aptamer sequences (Figure 3A). The CTC release efficiency was evaluated by dividing the CTC counts released from the TP-multimarker chip by the counts of target cells initially captured by the chip. After incubation with DNase I, the captured target cells achieved release by enzyme digestion (Figure 3B), and almost 80% of captured target cells were released from the chips, approximately 34% higher than the Aptamer chip undergoing the same treatment (Figure 3C). Due to the reasonable spatial structures on the interface, the interchain entanglement reduced effectively and DNase I was more accessible to the aptamer. Moreover, this release strategy works on the aptamer strands rather than the proteins expressed on the surface of the cell membrane so that most of the released cells (90.42%) remain viable (Figures 3D, S8).

Clinical Sample Analysis. Based on the above results, blood samples from breast cancer patients were used to investigate the clinical application of the TP-multimarker chip for CTC isolation. The whole blood samples were received from the First Affiliated Hospital of Sun Yat-Sen University with informed consent. Having been pretreated immediately,

https://doi.org/10.1021/acssensors.1c02692
ACS Sens. 2022, 7, 666−673

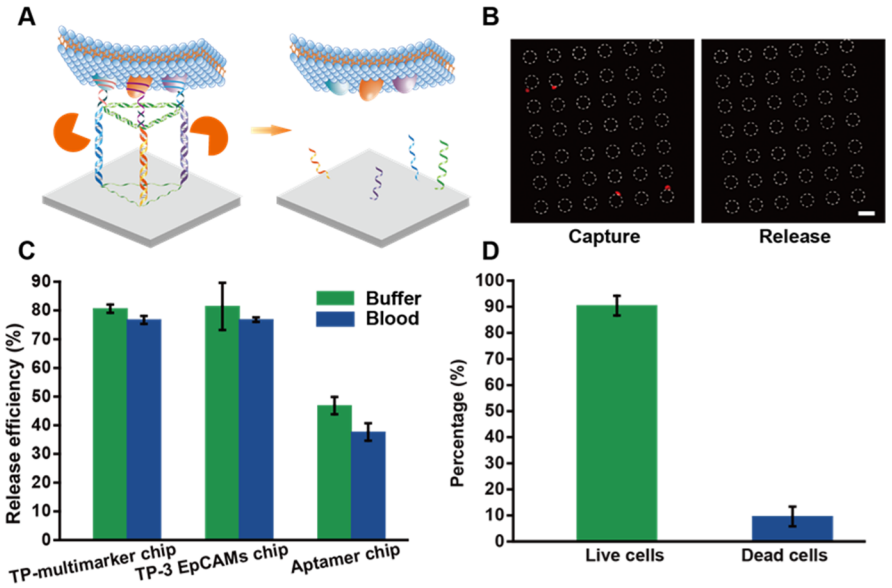

Figure 3. (A) Schematic diagrams of cell release. (B) Representative images of MCF-7 (red) captured on the TP-multimarker chip before and after DNase I treatment; scale bar = 50 μm. (C) Release efficiency of captured model cells MFC-7 using the TP-multimarker chip, TP-3EpCAMs chip, and Aptamer chip. (D) Cell viability of recovered MCF-7.

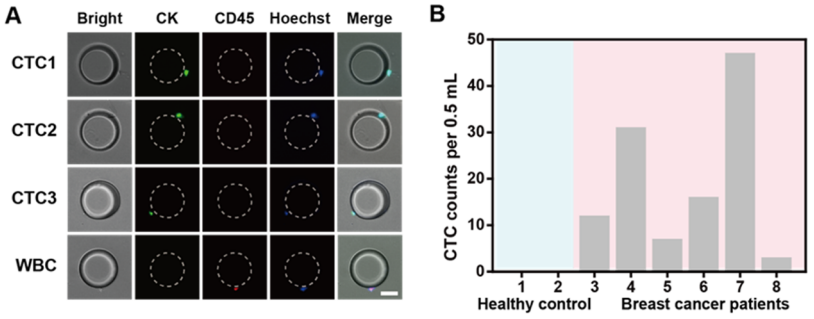

Figure 4. Clinical application of the TP-multimarker. (A) Representative immunofluorescence staining images of CTCs and white blood cells isolated from clinical samples (Hoechst+/CK+/CD45-for CTCs and Hoechst+/CK-/CD45 + for WBCs). Scale bar = 20 μm. (B) Quantification of the CTCs in the whole blood of 0.5 mL from two healthy people (1−2) and six breast cancer patients (3−8).

whole blood samples were injected into the chips and the isolated cells were identified via cell morphology and three-color immunocytochemistry. As shown in Figure 4A, cells were identified as CTCs if they showed a positive signal from the nuclear fluorophore (Hoechst 33342) and the epithelial marker cytokeratin (CK) but negative for CD45, whereas cells negative for Hoechst 33342 and CD45 but negative for CK were identified as WBCs. The number of CTCs in all six breast cancer patients ranged from 3 to 47 per 0.5 mL of blood, whereas no signs of CTCs were detected in samples from two healthy donors (Figure 4B; Table S2). The successful capture of CTCs from clinical samples demonstrates that the multivalent and ordered aptamer recognition interface endows an excellent performance of the TP-multimarker chip in the liquid biopsy field.

CONCLUSIONS

In this work, we demonstrated the feasibility of isolated CTCs from patients' blood samples with improved purity and molecule integrality. Using a TP-multimarker chip through an aptamer multimarker cocktail and the ordered spatial structure guided by frame nucleic acids, the engineered anisotropic recognition interface in a microfluidic chip has provided an effective strategy to improve ligand anchoring on the heterogeneous CTC surface, exhibiting excellent capture ability for high EpCAM expression cells as well as triple-negative breast cancer cells. In addition, the TP-multimarker chip has shown to be useful in detecting CTC in the clinical setting. Furthermore, owing to the modular design of the DNA nanostructure, the nanoplatform could allow turning the size of the recognition unit and the type of aptamers to achieve specific recognition of different cell phenotypes of CTCs, with a deeper understanding of protein distribution on the cell membrane. This strategy can be used in a wide variety of fields, including noninvasive cancer diagnosis and the detection of various biomarkers.

EXPERIMENTAL SECTION

Cell Lines and Reagents. The details for cell lines and reagents are listed in the Supporting Information.

Assembly and Characterization of the TPs. All DNA oligonucleotides were diluted to 100 μM in TE buffer (10 mM Tris−HCl, 1 mM EDTA, pH 8.0) and stored at −20 °C. To prepare a DNA TP, three DNA oligonucleotides (S1, S2, and S3) were mixed in an equimolar ratio in TM buffer (20 mM Tris, 50 mM $MgSO_4$, pH 8.0) at a final concentration of 1 μM. The TP was self-assembled by a slow cooling process from 95 to 4 °C. TP-3EpCAMs and the TP-

https://doi.org/10.1021/acssensors.1c02692
ACS Sens. 2022, 7, 666−673

multimarker were prepared under the same conditions. The formed DNA nanostructures were stored at 4 °C before use.

In this work, assembled products were characterized by agarose gel electrophoresis. 3% agarose gels were prepared in 1× TBE buffer (89 mM Trisboric, 2 mM EDTA, pH 8.0) and stained with YeaRed Nucleic Acid Gel Stain. DNA samples (10 μL, 1 μM) were mixed with 2 μL of 6× loading buffer. Electrophoresis was carried out in fresh 1× TBE buffer at 110 V for 60 min with an ice-water bath. For AFM imaging of the TP nanostructure, 20 μL of 2.5 nM TP was first added onto the surface of fresh mica and incubated for 10 min. Then, the mica was washed with TM buffer. Finally, 50 μL of the TM buffer was added to the mica surface, and AFM imaging was performed in the liquid-phase model with a Dimension FastScan (Bruker Santa Barbara, US) and SNL-10 probes.

Chip Fabrication and Modification. The functional chips were fabricated by assembling DNA nanostructures on a DLD-patterned microfluidic chip (DLD-Chip). The DLD-Chips were fabricated based on previous literature.[23] Briefly, the flow chamber was 35 mm long, 3.5 mm wide, and 30 μm high, and the circular micropillars were with 25 μm radius and 25 μm gaps. The tilt angle of the microarray was 3.2° to the fluid flow direction. Such array parametric combination enables more frequent interactions of cells greater than the critical diameter (DC ≈ 6 μm) and micropillars. The DLD channel was produced by standard soft lithography using an SU-8 mold on a silicon wafer. A 10:1 (w/w) PDMS premixture was poured onto a molded silicon wafer and cured in an 80 °C oven for 30 min; then, the curable PDMS was peeled off, with pouched inlets and outlets. The PDMS channel membrane and clean glass slide were activated by oxygen plasma and bonded together for 20 min.

Freshly prepared plasma-activated chips underwent gradual surface modification as follows: first, 4% (v/v in methanol) APTES was injected into the chip and incubated for 1 h. After being washed with ethanol and drying at 100 °C for 1 h, the amino-functionalized chip continued to react with a solution of 1 mM MBS and incubated for 1 h. After being washed with PBS, 1 μM TP nanostructure or Aptamer-EpCAM was added immediately and incubated for 2 h. All modification steps were performed at room temperature unless otherwise specified.

Cell Capture and Release Assay. Before capture, the chips were blocked with a blocking buffer (1× PBS with 5% BSA and 0.05% Tween 20) for 2 h to decrease nonspecific adsorption. The model cells MCF-7 and MDA-MB-231 were stained with membrane probe DiI, while Jurkat cells were stained with DiO. A certain number of labeled cells were scattered among 10^5 Jurkat cells and resuspended in PBS buffer or whole blood. Then, the artificial blood samples were injected into the microfluidic chip at a flow rate of 0.2 mL/h. After the cells were injected into the chip, PBS buffer was continued for another 10 min to flush out uncaptured cells. Subsequently, the captured cells were observed and counted using a fluorescence microscope (IX-83, Olympus). The capture efficiency could be defined as the percentage of the captured cells in the initial total cells.

For cell release, 50 U/mL DNase I was injected into the chip and incubated for 30 min at 37 °C. After being washed with PBS buffer at a high flow rate of 2 mL/h, the released cells were collected into a 32-well plate. Cells remaining in the chip were observed and counted using a fluorescence microscope again for evaluating the cells' release efficiency. Cell release efficiency was calculated as the percentage of the released cells in the captured cells. All experiments were performed three times.

Whole blood was collected from healthy people and should be processed immediately as soon as possible. After centrifugation at 800*g* for 10 min, the supernatant of serum was substituted by the same volume of PBS buffer. The artificial samples were fabricated by spiking a certain number of DiI-labeled MCF-7 or MDA-MB-231 cells into whole blood samples. The artificial samples were subjected to the capture-release assay as aforementioned.

Cell Viability Assay. After the capture-release assay, the recovered cells were stained with calcein-AM at 37 °C for 20 min. Subsequently, cells were imaged with two different wavelengths of laser beams (495 nm for calcein-AM and 549 nm for DiI) using a fluorescence microscope. DiI-labeled total cells and calcein AM-stained live cells were counted by Image J, and the cell viability rate was calculated by the following equation

$$\frac{\text{cell number(calcein} - \text{AM positive)}}{\text{cell number(DiI positive)}} \times 100\%$$

Detection of CTCs in Clinical Samples. Samples were taken from both healthy and breast cancer patients and handled within 12 h. After capture and washing, the CTCs captured on the chip were identified by common three-color immunocytochemistry. Briefly, cells on the chips were fixed with 4% polyformaldehyde solution for 10 min; then, the cells were permeabilized with Immunostaining Permeabilization Buffer Saponin for 10 min and blocked with 1% BSA for 40 min, followed by immunofluorescence staining with Hoechst 33 342, anti-human CD45, and anti-human CK. The immunofluorescence results were imaged on a fluorescence microscope, and cells with a staining profile of DAPI+/CD45-/CK+ were identified as CTCs. All included patients gave oral and written informed consent. The study was approved by the Institutional Review Board (IRB) of Sun Yat-sen University (IRB approval 2019-L054-1).

■ ASSOCIATED CONTENT

Supporting Information

The Supporting Information is available free of charge at https://pubs.acs.org/doi/10.1021/acssensors.1c02692.

Details on cell lines and reagents, assembly and characterization of DNA nanostructures, agarose gel electrophoresis analysis, AFM images of the TP multimarker, fluorescence microscopy images of the TP nanostructured chip and DiI-labeled target cells, optimization of the flow rate, cell capture yield toward WBCs, and fluorescence images of cell viability, DNA sequences for the assembly of DNA nanostructures, and data on the number of CTCs captured from breast cancer patients' blood samples (PDF)

■ AUTHOR INFORMATION

Corresponding Authors

Yuanqing Zhang − *School of Pharmaceutical Sciences, Sun Yat-sen University, Guangzhou 510006, China;* orcid.org/0000-0002-8761-5328; Email: zhangyq65@mail.sysu.edu.cn

Lingling Shui − *Joint Laboratory of Optofluidic Technology and Systems, South China Academy of Advanced Optoelectronics and Guangdong Provincial Key Laboratory of Nanophotonic Functional Materials and Devices, School of Information and Optoelectronic Science and Engineering, South China Normal University, Guangzhou 510006, China;* orcid.org/0000-0001-8517-1535; Email: shuill@m.scnu.edu.cn

Authors

Yan Liu − *Joint Laboratory of Optofluidic Technology and Systems, South China Academy of Advanced Optoelectronics, South China Normal University, Guangzhou 510006, China*

Zhun Lin − *School of Pharmaceutical Sciences, Sun Yat-sen University, Guangzhou 510006, China*

Ziwei Zheng − *School of Pharmaceutical Sciences, Sun Yat-sen University, Guangzhou 510006, China*

Complete contact information is available at: https://pubs.acs.org/10.1021/acssensors.1c02692

Notes

The authors declare no competing financial interest.

■ ACKNOWLEDGMENTS

This work was supported by the National Natural Science Foundation of China (82072087), the Key Technologies Research and Development Program of China (2016YFA0201200), the Guangdong Natural Science Fund for Distinguished Young Scholars (2017A030306016), the Guangdong Province Basic and Applied Research Fund (no. 2019B1515120037), the Science and Technology Program of Guangzhou (N. 2019050001), and the Joint Research Lab of Device Integrated Responsive Materials. The platforms of PCSIRT Project (no. IRT_17R40) and the MOE International Laboratory for Optical Information Technologies are also appreciated for providing technical support.

■ REFERENCES

(1) Weigelt, B.; Peterse, J. L.; van't Veer, L. J. Breast cancer metastasis: markers and models. *Nat. Rev. Cancer* **2005**, *5*, 591−602.
(2) Yoon, H. J.; Kozminsky, M.; Nagrath, S. Emerging role of nanomaterials in circulating tumor cell isolation and analysis. *ACS Nano* **2014**, *8*, 1995−2017.
(3) Alix-Panabières, C.; Pantel, K. Challenges in circulating tumour cell research. *Nat. Rev. Cancer* **2014**, *14*, 623−631.
(4) Loeian, M. S.; Aghaei, S. M.; Farhadi, F.; Rai, V.; Yang, H. W.; Johnson, M. D.; Aqil, F.; Mandadi, M.; Rai, S. N.; Panchapakesan, B. Liquid biopsy using the nanotube-CTC-chip: capture of invasive CTCs with high purity using preferential adherence in breast cancer patients. *Lab Chip* **2019**, *19*, 1899−1915.
(5) Wang, Z.; Qin, W.; Zhuang, J.; Wu, M.; Li, Q.; Fan, C.; Zhang, Y. Virus-Mimicking Cell Capture Using Heterovalency Magnetic DNA Nanoclaws. *ACS Appl. Mater. Interfaces* **2019**, *11*, 12244−12252.
(6) Wu, L.-L.; Zhang, Z.-L.; Tang, M.; Zhu, D.-L.; Dong, X.-J.; Hu, J.; Qi, C.-B.; Tang, H.-W.; Pang, D.-W. Spectrally Combined Encoding for Profiling Heterogeneous Circulating Tumor Cells Using a Multifunctional Nanosphere-Mediated Microfluidic Platform. *Angew. Chem., Int. Ed. Engl.* **2020**, *59*, 11240−11244.
(7) Murlidhar, V.; Rivera-Baez, L.; Nagrath, S. Affinity Versus Label-Free Isolation of Circulating Tumor Cells: Who Wins? *Small* **2016**, *12*, 4450−4463.
(8) Dong, J.; Chen, J.; Smalley, M.; Zhao, M.; Ke, Z.; Zhu, Y.; Tseng, H. R. Nanostructured Substrates for Detection and Characterization of Circulating Rare Cells: From Materials Research to Clinical Applications. *Adv. Mater.* **2020**, *32*, 1903663.
(9) Yu, M.; Bardia, A.; Wittner, B. S.; Stott, S. L.; Smas, M. E.; Ting, D. T.; Isakoff, S. J.; Ciciliano, J. C.; Wells, M. N.; Shah, A. M.; et al. Circulating breast tumor cells exhibit dynamic changes in epithelial and mesenchymal composition. *Science* **2013**, *339*, 580−584.
(a) Kling, J. Beyond counting tumor cells. *Nat. Biotechnol.* **2012**, *30*, 578−580. (b) Poellmann, M. J.; Nair, A.; Bu, J.; Kim, J. K. H.; Kimple, R. J.; Hong, S. Immunoavidity-Based Capture of Tumor Exosomes Using Poly(amidoamine) Dendrimer Surfaces. *Nano Lett.* **2020**, *20*, 5686. (c) Park, M.-H.; Reátegui, E.; Li, W.; Tessier, S. N.; Wong, K. H. K.; Jensen, A. E.; Thapar, V.; Ting, D.; Toner, M.; Stott, S. L.; et al. Enhanced Isolation and Release of Circulating Tumor Cells Using Nanoparticle Binding and Ligand Exchange in a Microfluidic Chip. *J. Am. Chem. Soc.* **2017**, *139*, 2741−2749.
(10) Zhu, L.; Lin, H.; Wan, S.; Chen, X.; Wu, L.; Zhu, Z.; Song, Y.; Hu, B.; Yang, C. Efficient Isolation and Phenotypic Profiling of Circulating Hepatocellular Carcinoma Cells via a Combinatorial-Antibody-Functionalized Microfluidic Synergetic-Chip. *Anal. Chem.* **2020**, *92*, 15229−15235. (a) Sun, N.; Lee, Y.-T.; Kim, M.; Wang, J. J.; Zhang, C.; Teng, P. C.; Qi, D.; Zhang, R. Y.; Tran, B. V.; Lee, Y. T.; et al. Covalent Chemistry-Mediated Multimarker Purification of Circulating Tumor Cells Enables Noninvasive Detection of Molecular Signatures of Hepatocellular Carcinoma. *Adv. Mater. Technol.* **2021**, *6*, 2001056. (b) Giannelli, G.; Koudelkova, P.; Dituri, F.; Mikulits, W. Role of epithelial to mesenchymal transition in hepatocellular carcinoma. *J. Hepatol.* **2016**, *65*, 798−808.
(11) Zhu, Y.; Zou, C.; Zhang, J.; Jiang, W. T.; Guan, F. L.; Tang, K. J.; Li, S. H.; Li, G. N.; Wang, J. H.; Ke, Z. F. Dynamically Monitoring the Clonal Evolution of Lung Cancer Based on the Molecular Characterization of Circulating Tumor Cells Using Aptamer Cocktail-Modified Nanosubstrates. *ACS Appl. Mater. Interfaces* **2020**, *12*, 5671−5679.
(12) Zhang, Z.; Liu, Q.; Tan, J.; Zhan, X.; Liu, T.; Wang, Y.; Lu, G.; Wu, M.; Zhang, Y. Coating with flexible DNA network enhanced T-cell activation and tumor killing for adoptive cell therapy. *Acta Pharm. Sin. B* **2021**, *11*, 1965−1977.
(13) Gao, Q.; Zhao, Y.; Xu, K.; Zhang, C.; Ma, Q.; Qi, L.; Chao, D.; Zheng, T.; Yang, L.; Han, D.; et al. Highly Specific, Single-step Cancer Cell Isolation with Multi-Aptamer-Mediated Proximity Ligation on Live Cell Membranes. *Angew. Chem., Int. Ed. Engl.* **2020**, *59*, 23564.
(14) Dunn, M. R.; Jimenez, R. M.; Chaput, J. C. Analysis of aptamer discovery and technology. *Nat. Rev. Chem.* **2017**, *1*, 76.
(15) Song, Y.; Shi, Y.; Huang, M.; Wang, W.; Wang, Y.; Cheng, J.; Lei, Z.; Zhu, Z.; Yang, C. Bioinspired Engineering of a Multivalent Aptamer-Functionalized Nanointerface to Enhance the Capture and Release of Circulating Tumor Cells. *Angew. Chem., Int. Ed. Engl.* **2019**, *58*, 2236−2240.
(16) Su, S.; Ma, J.; Xu, Y.; Pan, H.; Zhu, D.; Chao, J.; Weng, L.; Wang, L. Electrochemical Analysis of Target-Induced Hairpin-Mediated Aptamer Sensors. *ACS Appl. Mater. Interfaces* **2020**, *12*, 48133.
(17) Zhang, J.; Lin, B.; Wu, L.; Huang, M.; Li, X.; Zhang, H.; Song, J.; Wang, W.; Zhao, G.; Song, Y.; et al. DNA Nanolithography Enables a Highly Ordered Recognition Interface in a Microfluidic Chip for the Efficient Capture and Release of Circulating Tumor Cells. *Angew. Chem., Int. Ed.* **2020**, *59*, 14115−14119.
(18) Pei, H.; Zuo, X.; Zhu, D.; Huang, Q.; Fan, C. Functional DNA nanostructures for theranostic applications. *Acc. Chem. Res.* **2014**, *47*, 550−559.
(19) Qin, W.; Chen, L.; Wang, Z.; Li, Q.; Fan, C.; Wu, M.; Zhang, Y. Bioinspired DNA Nanointerface with Anisotropic Aptamers for Accurate Capture of Circulating Tumor Cells. *Adv. Sci.* **2020**, *7*, 2000647.
(20) Wunsch, B. H.; Smith, J. T.; Gifford, S. M.; Wang, C.; Brink, M.; Bruce, R. L.; Austin, R. H.; Stolovitzky, G.; Astier, Y. Nanoscale lateral displacement arrays for the separation of exosomes and colloids down to 20 nm. *Nat. Nanotechnol.* **2016**, *11*, 936−940.
(21) Lin, M.; Wang, J.; Zhou, G.; Wang, J.; Wu, N.; Lu, J.; Gao, J.; Chen, X.; Shi, J.; Zuo, X.; et al. Programmable engineering of a biosensing interface with tetrahedral DNA nanostructures for ultrasensitive DNA detection. *Angew. Chem., Int. Ed. Engl.* **2015**, *54*, 2151−2155.
(22) Song, T.; Shah, S.; Bui, H.; Garg, S.; Eshra, A.; Fu, D.; Yang, M.; Mokhtar, R.; Reif, J. Programming DNA-Based Biomolecular Reaction Networks on Cancer Cell Membranes. *J. Am. Chem. Soc.* **2019**, *141*, 16539−16543.
(23) Liu, Z. B.; Huang, F.; Du, J. H.; Shu, W. L.; Feng, H. T.; Xu, X. P.; Chen, Y. Rapid isolation of cancer cells using microfluidic deterministic lateral displacement structure. *Biomicrofluidics* **2013**, *7*, 011801.
(24) Nakatsuka, N.; Yang, K. A.; Abendroth, J. M.; Cheung, K. M.; Xu, X.; Yang, H.; Zhao, C.; Zhu, B.; Rim, Y. S.; Yang, Y.; et al. Aptamer-field-effect transistors overcome Debye length limitations for small-molecule sensing. *Science* **2018**, *362*, 319−324.
(25) Arteaga, C. L.; Sliwkowski, M. X.; Osborne, C. K.; Perez, E. A.; Puglisi, F.; Gianni, L. Treatment of HER2-positive breast cancer: current status and future perspectives. *Nat. Rev. Clin. Oncol.* **2011**, *9*, 16−32.
(26) Dong, J.; Jan, Y. J.; Cheng, J.; Zhang, R. Y.; Meng, M.; Smalley, M.; Chen, P. J.; Tang, X.; Tseng, P.; Bao, L.; et al. Covalent chemistry on nanostructured substrates enables noninvasive quantification of

https://doi.org/10.1021/acssensors.1c02692
ACS Sens. 2022, 7, 666−673

gene rearrangements in circulating tumor cells. *Sci. Adv.* **2019**, *5*, No. eaav9186.
(27) Poudineh, M.; Labib, M.; Ahmed, S.; Nguyen, L. N. M.; Kermanshah, L.; Mohamadi, R. M.; Sargent, E. H.; Kelley, S. O. Profiling Functional and Biochemical Phenotypes of Circulating Tumor Cells Using a Two-Dimensional Sorting Device. *Angew. Chem., Int. Ed.* **2017**, *56*, 163−168.
(28) Shen, Q.; Xu, L.; Zhao, L.; Wu, D.; Fan, Y.; Zhou, Y.; OuYang, W.; Xu, X. C.; Zhang, Z.; Song, M.; et al. Specific Capture and Release of Circulating Tumor Cells Using Aptamer-Modified Nanosubstrates. *Adv. Mater.* **2013**, *25*, 2368−2373.

https://doi.org/10.1021/acssensors.1c02692
ACS Sens. 2022, 7, 666−673